05,11

Magnetostructural features of phase transitions in the $Mn_{1-x}Co_xNiGe$ system Part 1. Experimental results

© V.I. Mitsiuk[1], G.S. Rimskiy[1], K.I. Yanushkevich[1], V.V. Koledov[2], A.V. Mashirov[2], V.I. Val'kov[3], A.V. Golovchan[3], O.E. Kovalev[3]

[1] Scientific and Practical Materials Research Center, National Academy of Sciences of Belarus, Minsk, Belarus
[2] Kotelnikov Institute of Radio Engineering and Electronics, Russian Academy of Sciences, Moscow, Russia
[3] Galkin Donetsk Institute for Physics and Engineering, Donetsk, DPR, Russia

E-mail: valkov09@gmail.com

Received June 23, 2021
Revised August 2, 2021
Accepted August 11, 2021

Experimental studies of the magnetic and structural properties of solid solutions of the $Mn_{1-x}Co_xNiGe$ system in a wide range of Co concentrations ($0.05 \le x \le 0.8$), temperatures ($5\,K \le x \le 600\,K$) and magnetic fields ($0.016\,T \le x \le 13.5\,T$) have revealed a number of nontrivial magnetic and magnetocaloric features of this system. The latter include: 1) a change in the nature of magnetic phase transitions from magnetostructural transitions of the 1st order paramagnetism-antiferromagnetism ($0.05 \le x \le 0.15$) to isostructural transitions of the 2nd order paramagnetism-ferromagnetism ($0.15 \le x \le 0.8$) with a change in the concentration of Co ; 2) anomalous behavior of low-temperature regions of magnetization in weak magnetic fields; 3) a change in the saturation magnetization and the appearance of irreversible magnetic field-induced transitions at helium temperatures in strong magnetic fields.

Keywords: irreversible magnetostructural first-order phase transition, helimagnetism, direct and inverse magnetocaloric effects.

DOI: 10.21883/PSS.2022.14.54333.153-1

1. Introduction

Practical interest in direct (DMCE) and inverse (IMCE) magnetocaloric effects [1–4], as a rule, accompanying magnetic phase transitions order−disorder and order−order, respectively, determines the relevance of the study of four-component alloys of type $Mn_{1-x}Cr_xNiGe$ [5], $MnNiGe_{1-x}Al_x$ [6], $MnNi_{1-x}Fe_xGe$ [7–9], $Mn_{1.9-x}Ni_xGe$ [10], $Mn_{1-x}Fe_xNiGe$ [11–12], $MnNi_{1-x}Co_xGe$ [13,14], $MnCo_{1-x}Cu_xGe$ [15]. In these systems, there is a structural phase transition of the displacement type $P6_3/mmc(\text{hex}) \leftrightarrow P_{\text{nma}}(\text{orth})$ [16,17] and a series of magnetic phase transitions. The „high-temperature" hexagonal phase has a Ni_2In type crystal structure ($P6_3/mmc$ symmetry group). The „low-temperature" rhombic phase has a TiNiSi type crystal structure (P_{nma} symmetry group). In the initial MnNiGe compound, an antiferromagnetic state arises in the rhombic phase, corresponding to the „soft" helimagnetic mode with the wave vector $\mathbf{q} = (0, 0, q_a)$ [18]. At doping, a ferromagnetic phase often appears and magnetic phase transitions disorder−order (PM−FM) and order−order (FM−AF) are formed, which have different magnetocaloric effects.

The $P6_3/mmc \leftrightarrow P_{\text{nma}}$ structural phase transition in the above germanides is a 1st order transition and can make an additional contribution to the magnetocaloric effect[9] when combined with a magnetic phase transition.

This work is devoted to experimental studies of the magnetic and crystalline properties of polycrystalline powders of solid-state solutions of the $Mn_{1-x}Co_xNiGe$ system using a static magnetic field with induction up to 14 T in a wide temperature range ($T = 5-600\,K$).

2. Methods of synthesis and research of samples

Polycrystalline powders of solid-state solutions of the $Mn_{1-x}Co_xNiGe$ system are synthesized by powder metallurgy from initial components. Powders taken in appropriate proportions were sintered in evacuated quartz ampoules in a single-zone resistance furnace. The furnace feed with the appropriate ratio of the initial components was slowly heated to a temperature of 1273 K, homogenized for 3 days, and quenched in ice water. The phase composition and unit cell parameters of the synthesized compositions were determined at room temperature by X-ray diffraction analysis using Cu$K\alpha$-radiation. The temperature dependences of the specific magnetization were studied in the temperature range of 80−600 K by the ponderomotive method in a magnetic field with induction $B = 0.8$ T. The

Table 1. Parameters a and c, lattice cell volume V, X-ray density at 293 K — $\rho_{X\text{-ray}}$, specific magnetization $\sigma_{80\,K}$ and magnetic moment $\mu_{80\,K}$ per formula unit at 80 K of $Mn_{1-x}Co_xNiGe$ solid-state solutions at 80 K, Curie temperature T_C

x	a, nm	c, nm	c/a	V, 10^{-2} m^3	$\rho_{X\text{-ray}}$, (g/cm^3)	$\sigma_{80\,K}$, A · m^2 · kg^{-1}	$\mu_{80\,K}$, μ_B	T_C, K
0.05	0.408_2	0.539_8	1.32	7.791	7.946	10.47	0.35	290*
0.10	0.408_1	0.537_4	1.32	7.749	7.998	29.16	0.97	237
0.15	0.406_9	0.534_3	1.31	7.664	8.096	38.68	1.29	193
0.20	0.407_3	0.532_7	1.31	7.652	8.117	30.60	1.02	170
0.30	0.406_7	0.528_9	1.30	7.577	8.216	12.60	0.42	134
0.40	0.405_4	0.522_3	1.29	7.448	8.375	3.46	0.12	–
0.50	0.404_4	0.519_1	1.28	7.352	8.503	1.72	0.06	–
0.60	0.402_7	0.514_9	1.28	7.233	8.661	1.45	0.05	–
0.70	0.401_3	0.511_4	1.27	7.134	8.800	1.41	0.05	–
0.80	0.399_8	0.508_9	1.27	7.045	8.930	1.35	0.05	–

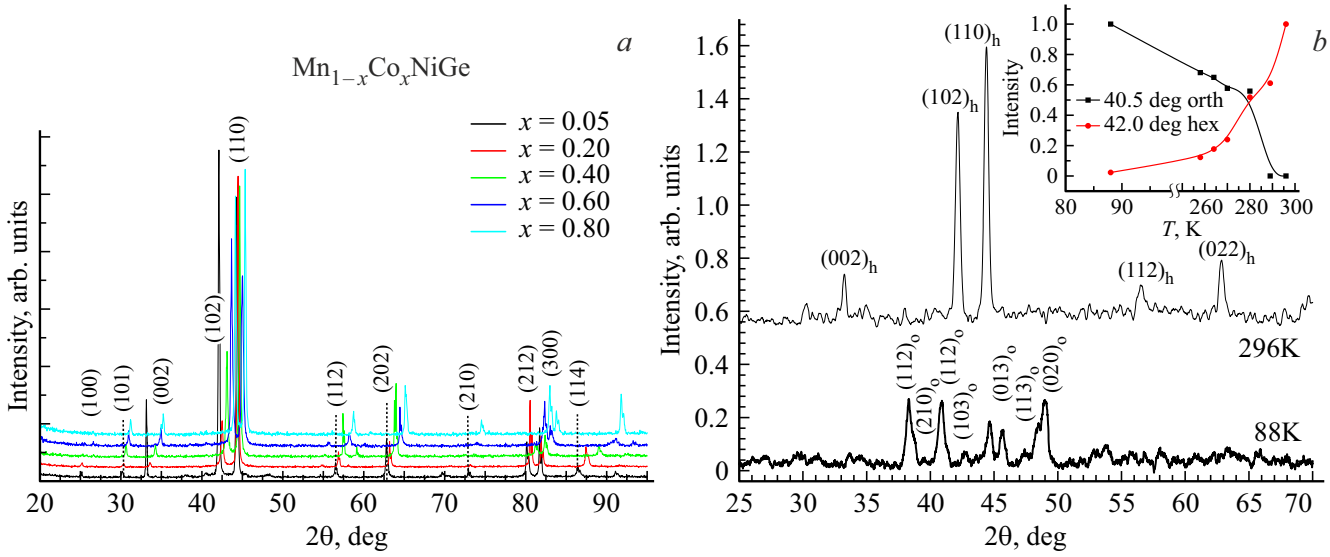

Figure 1. X-ray diffraction patterns of $Mn_{1-x}Co_xNiGe$ powders. a — room temperature ($T = 296$ K); b — $Mn_{0.95}Co_{0.05}NiGe$ at $T = 296$ K and at $T = 88$ K; the inset shows the temperature dependence of the intensity of the orthorhombic and hexagonal phases fractions at heating.

specific saturation magnetization and the parameters of the hysteresis loop of the specific magnetization of the powder samples were measured by the induction method on a vibrating magnetic meter in a magnetic field up to 14 T at temperatures of 5 K, 77 K. The temperature dependences of the specific magnetization were obtained during cooling and heating at a rate of 1.5 K/min in the temperature range of 5–300 K using a Cryogenics Lmtd magnetic meter in magnetic fields with induction $B = 0.016$; 0.1; 1; 5; 10; 13.5 T. To determine the isothermal change in entropy in the area of the phase transition, measurements of the magnetization in static fields up to 14 T were carried out. The magnetocaloric characteristics were calculated by an indirect method based on Maxwell's thermodynamic relations.

3. Results of X-ray and magnetometric measurements

X-ray studies of solid-state solutions of the $Mn_{1-x}Co_xNiGe$ system at room temperatures showed a hexagonal crystallographic structure of the Ni_2In type (space group $P6_3/mmc$) for the entire range of concentrations of Co ($x = 0.0.5$–0.80), Fig. 1, *a* under study. However, at cooling to nitrogen temperatures, the hexagonal structure remains stable only for samples with $x = 0.15$–0.80. In samples with $x = 0.05$–0.1, a decrease in temperature leads to the stabilization of a new crystal structure of the TiNiSi type (space group P_{nma}), Fig. 1, *b*. The process of temperature variation of the intensities of characteristic reflections in this case allows to state the presence of a structural 1st order phase transition of the

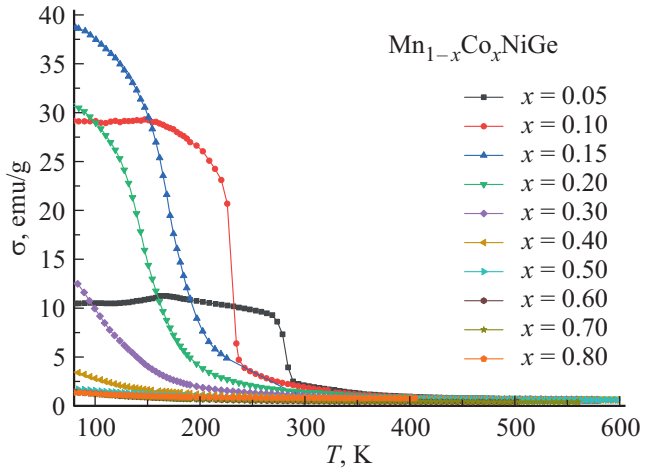

Figure 2. Temperature dependences of the magnetization of $Mn_{1-x}Co_xNiGe$ in a magnetic field of 0.86 T at heating.

displacement type $hex(P6_3/mmc) \leftrightarrow orth(P_{nma})$ [5,19] which results in the appearance of an rhombic phase with a crystal structure of the TiNiSi type, Fig. 1, *b*. This transition is accompanied by relatively large anisotropic changes in the lattice parameters and specific volume and corresponds to a diffuse 1st order phase transition $hex(P6_3/mmc) \leftrightarrow orth(P_{nma})$ characteristic of a number of solid-state solutions based on the MnNiGe compound.

Low-temperature diffraction patterns were obtained in Cu$K\alpha$-radiation using a low-temperature X-ray camera on a DRON-1.5 device. According to the data obtained, in the sample with $x = 0.15$ in the temperature range $T = 88-296$ K, the hexagonal phase is preserved, while in the sample with $x = 0.05$ below 290 K, there is the appearance of the orthorhombic phase (inset in Fig. 1, *b*).

Concentration dependences of parameters a, c and lattice cell volume V of $Mn_{1-x}Co_xNiGe$ solid-state solutions in

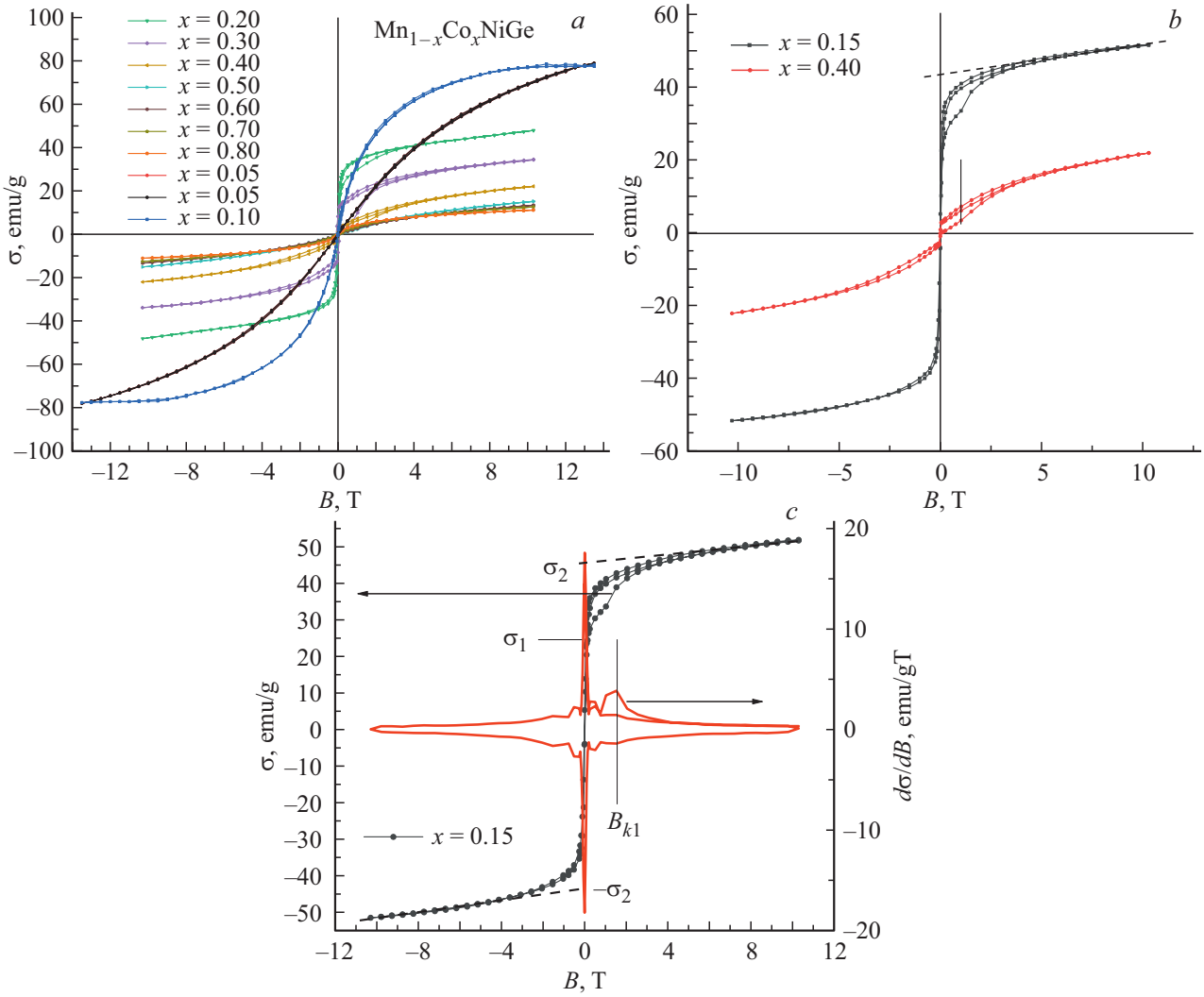

Figure 3. Field dependences of the magnetization of alloys of the $Mn_{1-x}Co_xNiGe$ system at $T = 5$ K. *a* — $(0 \le B \le 10\,T)$, *b* — irreversible magnetic field-induced order−order magnetic phase transitions in samples with reduced saturation magnetization; *c* — superposition of $\sigma(B)$ and $d\sigma(B)/dB$; B_{k1} — induction of the 1-th critical field of an irreversible induced order−order transition; *d* — field dependences of the magnetization at $T = 77$ K $(0 \le B \le 10\,T)$; *e* — field dependences of the magnetization at $T = 77$ K $(0 \le B \le 0.5\,T)$.

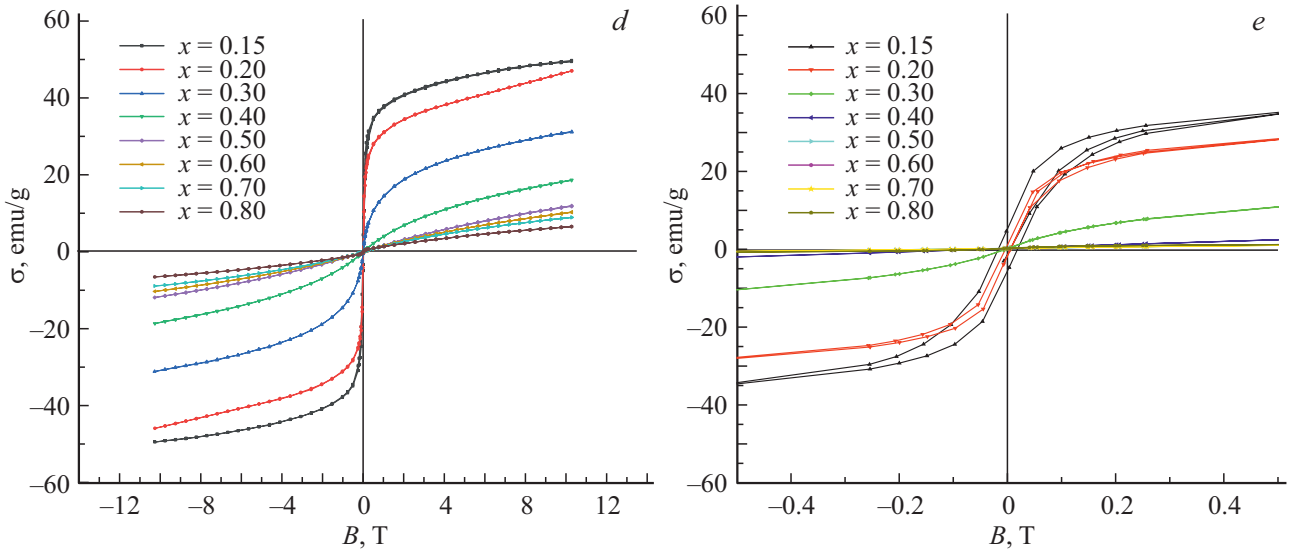

Fig. 3 (*contd.*).

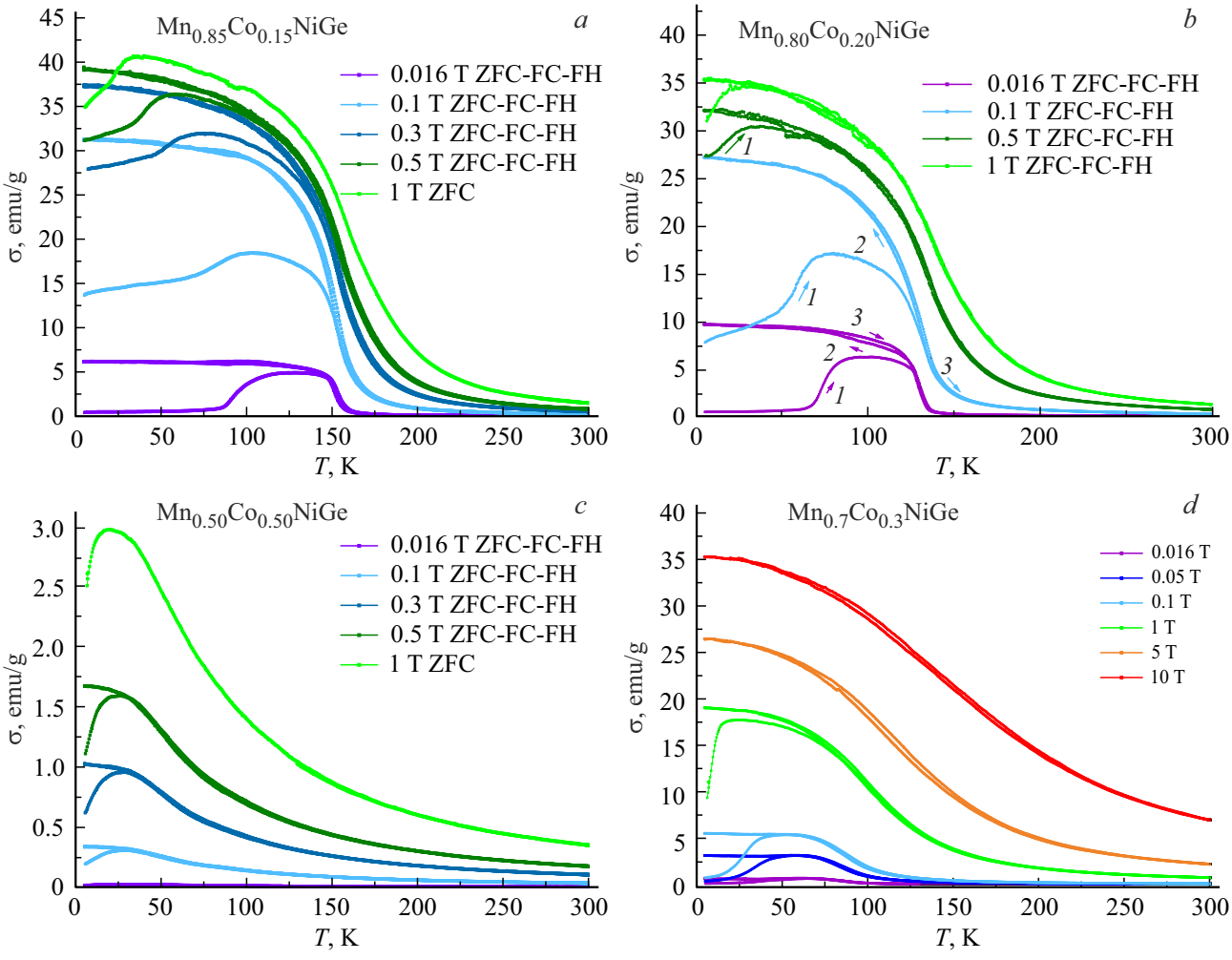

Figure 4. Temperature dependences of the magnetization of polycrystalline alloys of the $Mn_{1-x}Co_xNiGe$ system in weak magnetic fields.

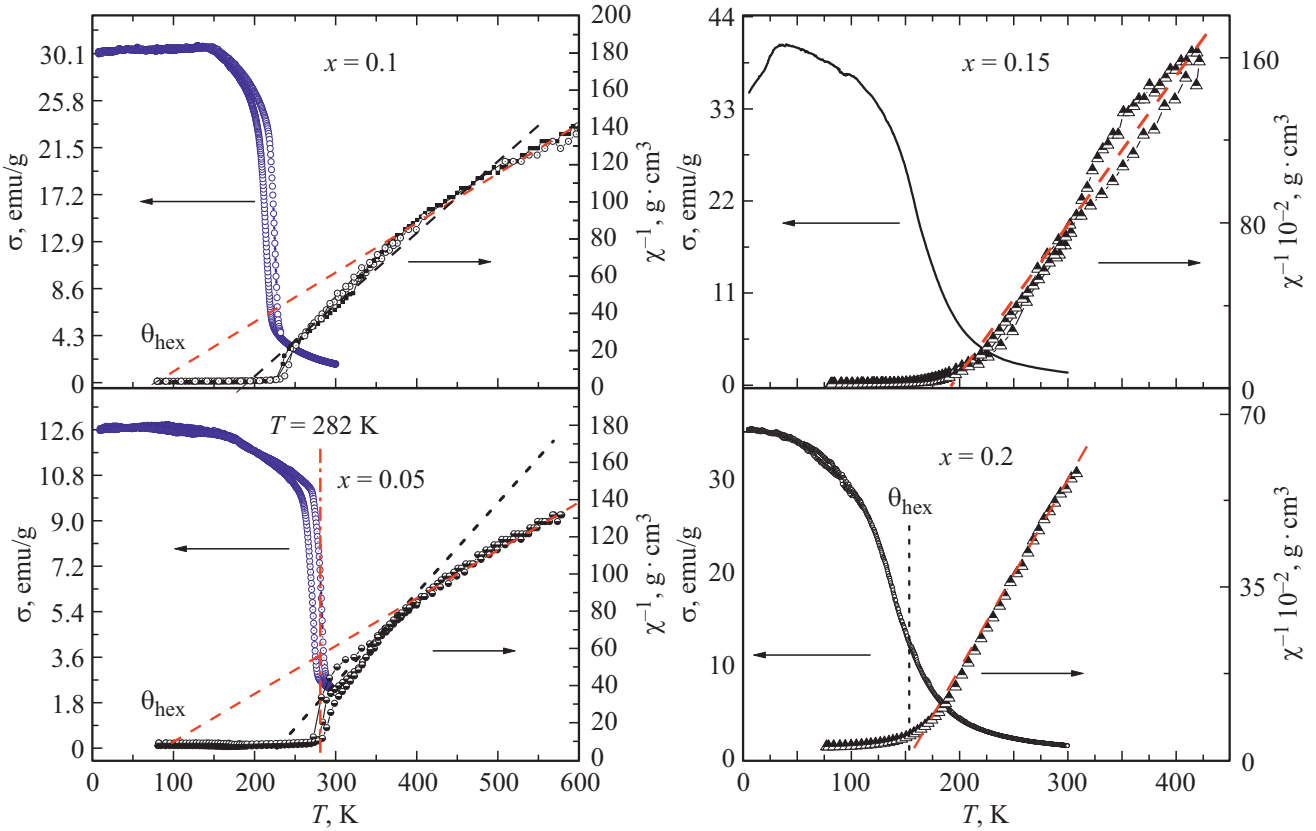

Figure 5. Combined temperature dependences of the inverse magnetic susceptibility $\chi^{-1}(T)$ in a field with induction $B = 0.86$ T and magnetization in a field with induction $B = 1$ T in some samples of the $Mn_{1-x}Co_xNiGe$ system.

which the cationic substitution of manganese for cobalt reaches up to 80 at.% are presented in Table 1.

The results of measurements of the specific magnetization of the studied compositions are shown in Fig. 2. Cationic substitution in the $Mn_{1-x}Co_xNiGe$ system already at 10% substitution of manganese for cobalt leads to violation of the antiferromagnetic ordering. At $x \geq 0.10$, solid-state solutions exhibit ferromagnetic properties.

Figure 3 shows the field dependences of the magnetization $\sigma(H)$ at temperatures 5 and 77 K, respectively. The specific retained magnetization (σ_r) and the coercive force (H_c) are determined as per these measurements. The saturation magnetization (m_s) expressed in Bohr magnetons per formula unit can be calculated by the formula

$$m_s = \frac{\sigma_s \cdot M}{5585},$$

where M — molar mass; 5585 — a value equal to the product of the Bohr magneton (μ_B) and the Avogadro number. The values obtained for the $Mn_{1-x}Co_xNiGe$ system at 5 and 77 K are given in Table 2.

Let us separately review the results of low-temperature (Fig. 4) and high-temperature (Fig. 5) measurements in magnetic fields with an induction of 0.1–1 T order.

Table 2. Specific retained magnetization (σ_r) and coercive force (H_c) of $Mn_{1-x}Co_xNiGe$ samples at temperatures 5 and 77 K

x	$T = 5$ K		$T = 77$ K	
	σ_r, A · m² · kg⁻¹	H_c, T	σ_r, A · m² · kg⁻¹	H_c, T
0.05	0.051	0.005	0.04	0.00175
0.10	0.32	0.00575	0.19	0.0038
0.15	6	0.0165	5.5	0.0175
0.20	5	0.0188	1.45	0.005
0.30	8.6	0.085	–	–
0.40	0.65	0.008	–	–
0.50	0.5	0.0165	–	–
0.60	0.11	0.0086	–	–
0.70	0.174	0.174	–	–
0.80	–	–	–	–

The results of high-temperature measurements of the magnetization in a field with induction $B = 0.86$ T give an idea of the features of the temperature dependence of the inverse paramagnetic susceptibility $\chi^{-1}(T)$. In Fig. 5, the dependences $\chi^{-1}(T)$ are superimposed with the temperature dependences of the magnetization $\sigma(T)$ measured in fields with induction up to 14 T.

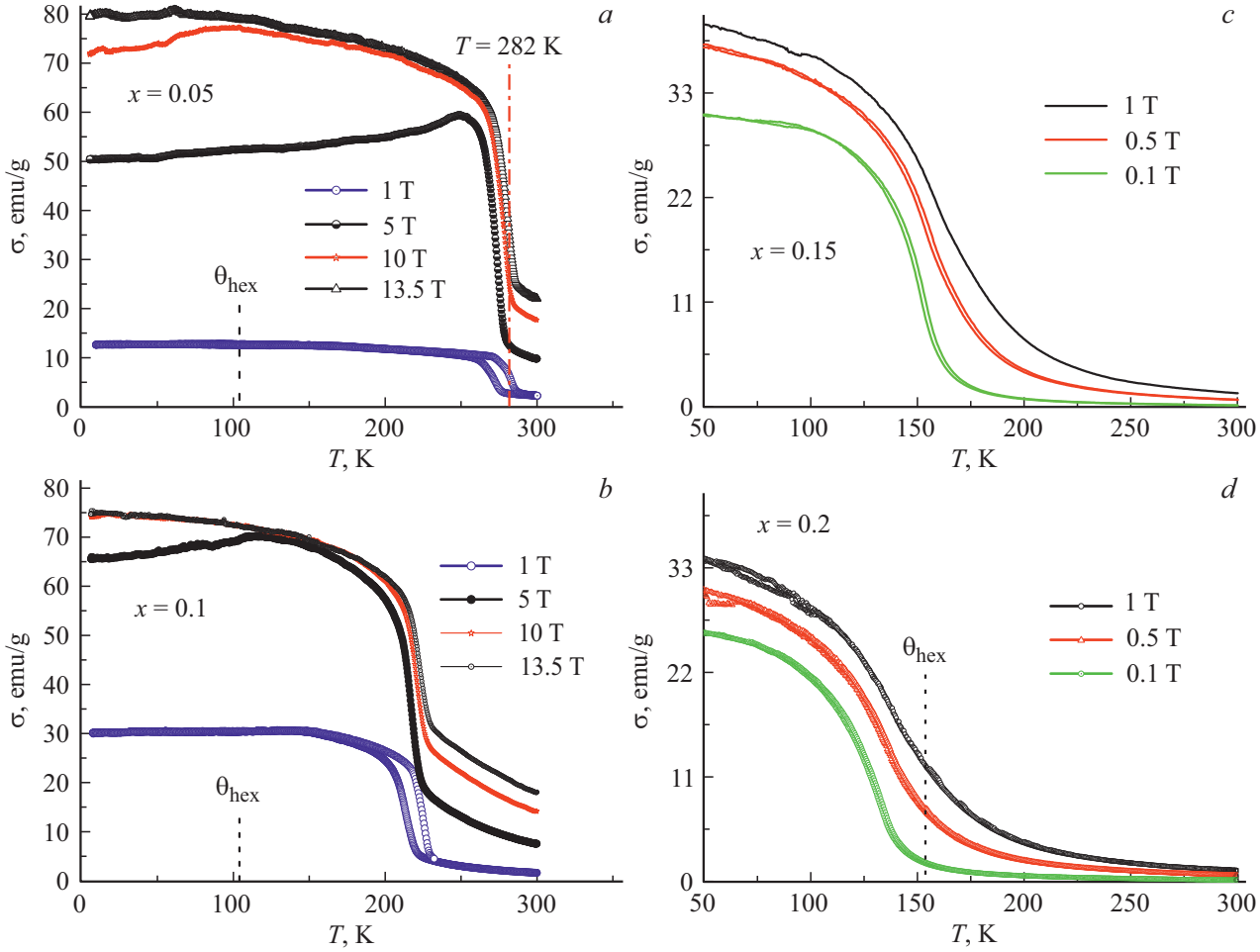

Figure 6. Temperature dependences of $\sigma(B)$ magnetization with different values of magnetic field induction in some alloys of the $Mn_{1-x}Co_xNiGe$ system.

Measurements of the temperature dependences of the magnetization in intense magnetic fields (Fig. 6) give an idea of the displacement of magnetic phase transitions by a field.

4. Magnetocaloric properties

The magnetocaloric properties of the investigated alloys were determined indirectly by calculation on the basis of Maxwell's thermodynamic relations from the magnetization curves (Fig. 7, 8).

5. Main conclusions from the experimental results

Based on X-ray and magnetic measurements, literature data [20], it can be concluded that at $x = 0.05-0.15$ in the $Mn_{1-x}Co_xNiGe$ system as the temperature decreases, there are magnetostructural phase transitions of the 1st order paramagnetism–antiferromagnetism (PM–AF). The high-temperature paramagnetic (PM) phase corresponds to the hexagonal crystal structure (hex) with the symmetry group $P6_3/mmc$. The low-temperature antiferromagnetic (AF) phase with a rhombic lattice (orth, symmetry group P_{nma}) presumably corresponds to the soft mode of the HM (orth) helicoidal structure. Therefore, it is quite easily deformed in a magnetic field and acquires a significant magnetization along its direction. The temperatures of magnetic ordering — T_1 (disordering — T_2) coincide with the temperatures of magnetostructural transitions PM(hex) $\leftrightarrow$ HM(orth).

Magnetostructural first-order transitions PM(hex) $\leftrightarrow$ HM(orth) are accompanied by temperature hysteresis, an anomalous behavior of inverse *PM* susceptibility $\chi^{-1}(T)$, characteristic of magnetostructural transitions (Fig. 5, *a, b*) [5] and are shifted in a magnetic field to higher temperatures, Fig. 6, *a, b*.

The field dependences $\sigma(B)$ measured in the vicinity of the temperature $T_m = 282\,K \leq T_C$ in Fig. 8 (dash-dotted line on the series of dependences $\sigma(T)$ for $x = 0.05$) show anomalous behavior, which is a sequence of two processes. The anhysteretic magnetization with increasing field induction B occurs up to $B_i \approx 4\,T$. With a further increase and subsequent decrease in the induction, the dependence $\sigma(B)$ exhibits hysteresis properties characteristic of reversible

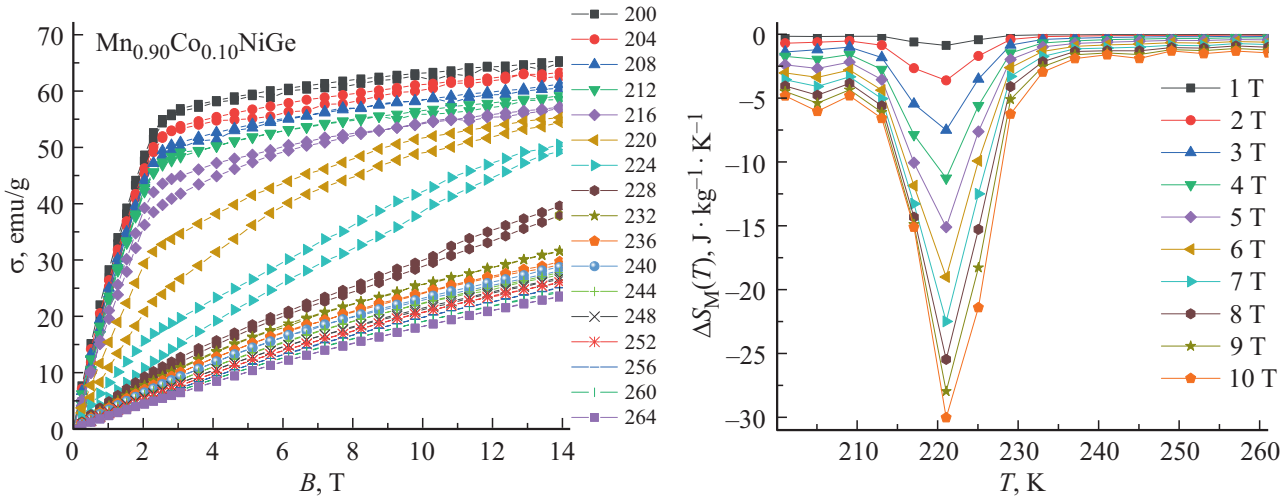

Figure 7. Isothermal changes in the magnetization and magnetic entropy in the $Mn_{0.90}Co_{0.10}NiGe$ solid-state solution with a change of induction in the magnetic field.

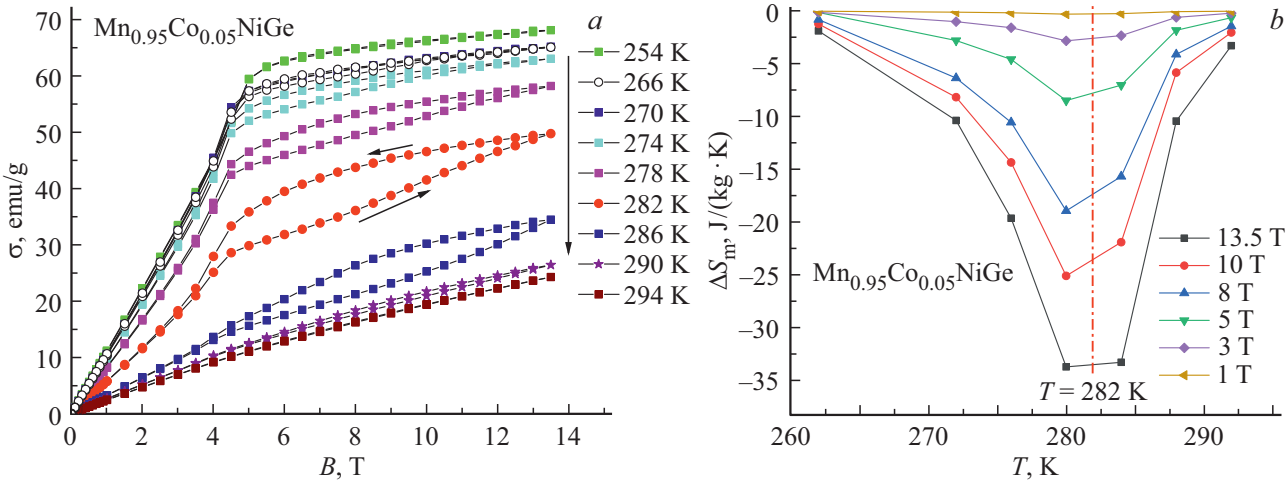

Figure 8. Isothermal changes in the magnetization and magnetic entropy in the $Mn_{0.95}Co_{0.05}NiGe$ solid-state solution.

magnetic field-induced first-order transitions PM ↔ FM, which are in a quenched sample of the related system $Mn_{1-x}Cr_xNiGe$ for $x = 0.11$ [19]. As the temperature decreases, the $\sigma(B)$ dependence in fields below B_i becomes steeper, the hysteresis properties in fields above B_i weaken and completely disappear below 266 K.

At helium temperatures (Fig. 3), the dependences $\sigma(B)$ for samples with $x \leq 0.1$ demonstrate a smooth anhysteretic increase in the magnetization up to 80 emu/g with a tendency to saturate in fields with induction over 10 T. Such behavior of $\sigma(B)$ dependencies is absolutely not typical for samples with $x = 0.15-0.8$.

For samples with a Co concentration in the range $x = 0.15-0.8$, the low-temperature $\sigma(B)$ dependences in Fig. 3 and in fields with an induction of over 4 T, on the one hand, demonstrate a clear tendency to saturation, characteristic of ferromagnetism. On the other hand, at helium temperatures, the $\sigma(B)$ dependences in fields up to 4 T can be interpreted as irreversible magnetic field-induced magnetic 1st order phase transitions order−order. This is clearly seen in the example of the combined dependences $\sigma(B)$ and $d\sigma(B)/dB = \sigma'_B(B)$ for a sample with $x = 0.15$, Fig. 3, *c*. The existence of the first critical field $B_{k1} = 2T$, in the area of a relatively sharp increase in magnetization and corresponding to the maximum of the dependence $\sigma'_B(B)$ at $B_{k1} \approx 2T$ as the induction increases and the conservation of the induced state after the reverse decrease in the induction (the absence of B_{k2}) explains what has been said. Meanwhile, the saturation magnetization of induced FM states for samples with $x = 0.15-0.8$ is more than 1.5 times less than the magnetization of the deformed helimagnetic state in samples with $x = 0.05-0.10$. Another distinctive feature of samples with $x = 0.15-0.8$ is the absence of hysteresis phenomena and abrupt changes in the temperature dependences of $\sigma(B)$, Fig. 6. This may be due to the isostructural nature of the magnetic ordering, which

is realized in samples with $x = 0.15-0.8$ as second-order isostructural transitions PM(hex) $\leftrightarrow$ FM(hex). In addition to direct X-ray measurements, this is evidenced by the absence of characteristic anomalies in the temperature dependences of the inverse susceptibility, Fig. 5 and literature data[20].

6. Conclusion

An integrated approach, including X-ray, magnetometric measurements in a wide range of magnetic field strengths and temperatures, made it possible to establish a number of magnetostructural and magnetocaloric features of polycrystalline samples of the $Mn_{1-x}Co_xNiGe$ system. The main features include two scenarios for the appearance of magnetic order at high temperatures with different saturation magnetizations in the low-temperature state and the presence of irreversible transitions induced by a magnetic field, accompanied by a relatively sharp increase in saturation magnetization.

The first one is realized in samples with $x < 0.15$, in which the structural transition of the 1st order $P6_3/mmc(\text{hex}) \leftrightarrow P_{\text{nma}}(\text{orth})$ coincides in weak magnetic fields with the appearance (disappearance) of helimagnetism HM(orth) $\leftrightarrow$ PM(hex). In intense magnetic fields, the magnetostructural ordering HM(orth) $\leftrightarrow$ PM(hex) transforms into a magnetostructural transition FM(orth) $\leftrightarrow$ PM(hex), accompanied by an abrupt change magnetization. In the temperature area of realization of this transition, the maximum MCE is reached.

The second scenario is realized in samples with $x \geq 0.15$, in which the magnetic disorder within the hexagonal structure corresponds to a second-order isostructural transition ferromagnetism–paramagnetism FM(hex) $\leftrightarrow$ PM(hex). Meanwhile, in the area of nitrogen temperatures, the anomalous sensitivity of the magnetization to the ZFC and FC modes in weak fields may indicate the presence of order–order magnetostructural transitions, presumably FM(hex) $\leftrightarrow$ HM(orth). In an intense magnetic field, this transition is suppressed, but the opportunity of its existence can be the cause of irreversible magnetic field-induced stick-slip increases in magnetization corresponding to the supposedly irreversible magnetostructural transition HM(orth) $\leftrightarrow$ FM(hex) that occurs during sample magnetization at low temperatures. This field-induced low-temperature transition may be the main driver of the relatively strong inverse magnetocaloric effect at helium temperatures.

Funding

The research was funded by the Belarusian Republican Foundation for Basic Research and the Russian Foundation for Basic Research as part of the scientific project No. T20P-204 and No. 20-58-00059 respectively.

Conflict of interest

The authors declare that they have no conflict of interest.

References

[1] S. Taskaev, V. Khovaylo, M. Ulyanov, D. Bataev, E. Danilova, D. Plakhotskiy. Key. Eng. Mater. **833**, 176 (2020).
[2] T. Numazawa, K, Kamiya, T. Utaki, K. Matsumoto. Supercond. Cryogenics **15**, 1 (2013).
[3] H. Zhang, R. Gimaev, B. Kovalev, K. Kamilov, V. Zverev, A. Tishin. Physica B **558**, 65 (2019).
[4] E.Z. Valiev. Fizika metallov i metallovedenie **104**, *1*, 12 (2007) (in Russian).
[5] V.I. Val'kov, A.V. Golovchan, V.V. Koledov, B.M. Todris, V.I. Mityuk. FTT **62**, *5*, 710 (2020) (in Russian).
[6] T. Samanta, I. Dubenko, A. Quetz, S. Temple, S. Stadler, N. Ali. Appl. Phys. Lett. **100**, *5*, 052404 (2012).
[7] K.A. Korolev, A.P. Sivachenko, I.F. Gribanov, A.V. Golovchan, V.I. Kamenev, T.S. Sivachenko, A.V. Mashirov, V.I. Mityuk, E.P. Andreichenko, S.V. Taskaev. Chelyabinskiy fiz.--mat. zhurn. **5**, *5*, 569 (2020) (in Russian).
[8] Z. Cheng-Liang, W. Dun-Hui, C. Jian, W. Ting-Zhi, X. Guang-Xi, Z. Chun. Chin. Phys. B **20**, 097501 (2011).
[9] E. Liu, W. Wang, L. Feng, W. Zhu, G. Li, J. Chen, H. Zhang, G. Wu, C. Jiang, H. Xu, F. Boer. Nature Commun. **3**, 873 (2012).
[10] C.L. Zhang, D.H. Wang, Q.Q. Cao, Z.D. Han, H.C. Xuan, Y.W. Du. Appl. Phys. Lett. **93**, 122505 (2008).
[11] G.S. Rimskiy, K.I. Yanushkevich, N.M. Belozerova, D.P. Kozlenko, A.V. Rutkauskas. FTT **63**, *3*, 393 (2021) (in Russian).
[12] K. Xu, Z. Li, E. Liu, H. Zhou, Y. Zhang, C. Jing. Sci. Rep. **7**, 41675 (2017).
[13] C. Zhang, D. Wang, Q. Cao, S. Ma, H. Xuan, Y. Du. J. Phys. D **43**, 205003 (2010).
[14] C.L. Zhang, J. Chen, T.Z. Wang, G.X. Xie, C. Zhu, D.H. Wang. Solid State Commun. **151**, 1359 (2011).
[15] H. Zhang, Y. Li, E. Liu, K. Tao, M. Wu, Y. Wang, H. Zhou, Y. Xue, C. Cheng, T. Yan, K. Long, Y. Long. Mater. Design **114**, 531 (2017).
[16] J.-T. Wang, D.-S. Wang, C. Chen, O. Nashima, T. Kanomata, H. Mizuseki, Y. Kawazoe. Appl. Phys. Lett. **89**, 262504 (2006).
[17] V. Johnson. Inorg. Chem. **14**, 1117 (1975).
[18] B. Penc, A. Hoser, S. Baran, A. Szytuła. Phase Transit. **91**, 118 (2018).
[19] V.I. Val'kov, V.I. Kamenev, A.V. Golovchan, I.F. Gribanov, V.V. Koledov, V.G. Shavrov, V.I. Mityuk, P. Duda. FTT **63**, *5*, 628 (2021) (in Russian).
[20] E.K. Liu, H.G. Zhang, G.Z. Xu, X.M. Zhang, R.S. Ma, W.H. Wang, J.L. Chen, H.W. Zhang, G.H. Wu, L. Feng, X.X. Zhangl. Appl. Phys. Lett. **102**, *12*, 122405 (2013).